LANGMUIR

Article

Weakly Ionically Bound Thermosensitive Hyperbranched Polymers

Hansol Lee, Alexandr Stryutsky, Akhlak-Ul Mahmood, Abhishek Singh, Valery V. Shevchenko, Yaroslava G. Yingling, and Vladimir V. Tsukruk*

Cite This: *Langmuir* 2021, 37, 2913−2927

Read Online

ACCESS | 📊 Metrics & More | 📰 Article Recommendations | 🅢🅘 Supporting Information

ABSTRACT: We synthesized novel amphiphilic hyperbranched polymers (HBPs) with variable contents of weakly ionically tethered thermoresponsive poly(N-isopropylacrylamide) (PNIPAM) macrocations in contrast to traditional covalent linking. Their assembling behavior was studied below and above the lower critical solution temperature (LCST). The HBPs underwent a morphological transition under changing temperature and ionic strength due to the LCST transition of PNIPAM and the reduction in the ionization degree of terminal ionic groups, respectively. We suggest that, in contrast to traditional branched polymers, ionically linked PNIPAM macrocations can reversibly disassociate from the sulfonate groups and form mobile coronas, endowing the dynamic micellar morphologies. In addition, assembly at the air−water interface confined PNIPAM macrocations and resulted in the formation of heterogeneous Langmuir−Blodgett (LB) monolayers with diverse surface morphologies for different peripheral compositions with circular domains formed in the condensed state. The HBPs with 25% PNIPAM showed larger and more stable circular domains that were partially preserved at high compression than those of HBPs with 50% PNIPAM. Moreover, the LB monolayers showed variable surface mechanical and surface charge distribution, which can be attributed to net dipole redistribution caused by the behavior of mobile PNIPAM macrocations and core sulfonate groups.
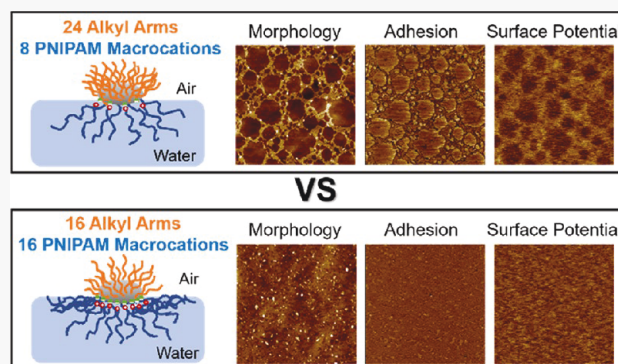
INTRODUCTION

Incorporating ionizable groups into macromolecular backbones is a known strategy for generating nanostructures that can change morphologies in response to variations in pH or ionic strength. In a polar solvent, the ionizable groups dissociate and leave behind a system of charged chains and counter ions that can be either bound or mobile. The association/dissociation of counter ions can thus be tuned in a wide range.[1,2] In particular, amphiphilic polyelectrolytes bearing ionizable groups as repeating units can dynamically respond to external stimuli, forming various morphologies, such as spherical, star-like/hairy, crew-cut, and cylindrical micelles, vesicles, lamellar mesophases, and micellar aggregates.[3−7] In addition to stimuli-responsive behavior, the interplay of electrostatic interactions with counter ion entropy and local solubility contributes to creating a diverse range of order/disordered morphologies, which are normally inaccessible to traditional nonionic polymers, by shifting traditional phase boundaries.[8−12] For instance, phase diagrams for linear polyelectrolyte block copolymers show gyroid or cylindrical phases with long-range continuity governed by ionic interactions.[13,14]

Branched polymers bearing multiple functionalities are promising candidates to realize polymer materials with preprogrammed complex morphologies and multifunctional properties. Branched polyelectrolytes with various architectures, such as brushes,[15,16] star copolymers,[17,18] and hyperbranched molecules,[19,20] were reported to show rich phase behavior and responsive micellar organization.[21−25] In contrast to linear polyelectrolytes, branched counterparts possess readily controlled diverse functionalities in cores, inner arms, and outer shells, which can promote the formation of complex morphologies with multifunctional responsive behavior.[26−29] For example, star polyelectrolytes composed of hydrophobic polystyrene (PS) arms and amphoteric poly(2-vinyl-pyridine)-b-poly(acrylic acid) (P2VP-b-PAA) arms formed various morphologies, such as unimolecular micelles, worm-like micelles, and network-like large assemblies. Their morphologies were determined by the location and pH-dependent conformations of the P2VP segment (inner) and PAA segment (outer).[30] Introducing large counter ions of a different nature can alter the functionality of outer shells, affect hydrophilic/hydrophobic balance, and induce stimuli-sensitive behav-
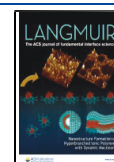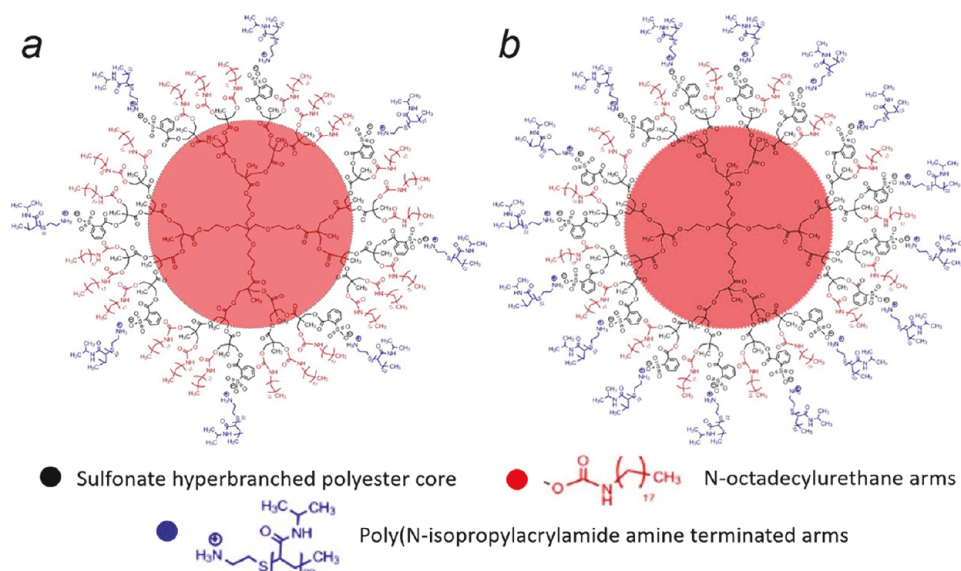
Figure 1. Chemical structures of ionically bound thermosensitive hyperbranched polymers: (a) S8P8 HBPs and (b) S16P16 HBPs.

ior.[31−35] For example, ionic dendrimers functionalized with hydrophobic fatty acids as counter ions self-assembled into micelles, lamellae, or nanospheres with a lamellar structure depending on the number of fatty acids linked to the dendrimer core.[32] In our recent study, we found that hyperbranched polymers (HBPs) with thermoresponsive poly(N-isopropylacrylamide) (PNIPAM) macrocations showed temperature-induced phase transformation controlled by the lower critical solution temperature (LCST) of PNIPAM macrocations.[33] Moreover, it has been demonstrated that the deposition of polyelectrolytes changes the surface charge of films and manipulates the film properties, such as water content and mobility, electrochemical charge transport, and electrocatalytic properties.[36−42] Although a plenty of studies have been reported on the control over surface properties using linear polyelectrolytes, branched polyelectrolytes have been relatively unexplored.[43,44]

In this work, we report the synthesis and assembling behavior of novel hyperbranched polymers functionalized with weakly ionically bound thermoresponsive chains as macro-counter ions. The macromolecules synthesized here are composed of hydrophobic polyester cores with variable peripheral chemical composition. Hydrophobic n-octadecylur-ethane arms and weakly tethered ionically bound hydrophilic macrocations are employed as peripheral components. The presence of mobile macrocations provides the HBPs with dynamic response characteristics, allowing for tuning the morphology of HBP assemblies by changing temperature and adding salts. In addition, strong vertical amphiphilicity-driven segregation at the air−water interface restricts PNIPAM macrocations in water, resulting in the formation of Langmuir monolayers of HBPs with diverse surface morphologies. Not only the surface morphology but also surface mechanical and surface charge distribution of the monolayers can be tuned by adjusting deposition conditions (e.g., temperature and surface pressure) and peripheral chemical composition.

■ EXPERIMENTAL SECTION

Synthesis of Materials. N-Octadecylisocyanate, 2-sulfobenzoic acid cyclic anhydride, and poly(N-isopropylacrylamide) amine terminated (M_n = 2500 g/mol) were purchased from Aldrich and used as received. Hyperbranched aliphatic polyester polyol Boltorn H30 (Perstorp) with molecular weight M_w = 3500 g/mol comprising 32 terminal OH groups in the outer shell was purified by precipitation of dimethylformamide (DMF) solution in diethyl ether followed by vacuum drying at 25−30 °C for 6 h (an equivalent molecular weight measured by hydroxyl groups via the acetylation technique is equal to 117 g/equivalent).[45] Phthalic anhydride was purified by sublimation, and all solvents were dried and distilled before use. Ultrapure water was obtained with a three-stage Millipore Milli-Q Plus 185 purification system (resistivity ≥18.2 MΩ·cm) (see more details in the Supporting Information).

**Assembly of Hyperbranched Polymers in Aqueous Media.** The aqueous assembly was carried out using the solvent-addition method.[46,47] Hyperbranched polymers were dissolved in tetrahy-drofuran (THF) at 50 mg/mL under stirring for 24 h at room temperature and then added to water dropwise at 1 mL/min. THF was evaporated under stirring for 24 h at room temperature, and the final concentration was 1 mg/mL.

For sample preparation, highly polished [100] silicon substrates (University Wafer) were cleaned with Piranha solution (2:1 concentrated sulfuric acid to hydrogen peroxide mixture, *caution: strong oxidizer!*) according to the common procedure.[27] The substrates were then thoroughly rinsed with ultrapure water and dried with dry nitrogen before deposition. A drop (5 μL) of hyperbranched polymer solution was placed onto the precleaned silicon substrate and air-dried. For preparing samples above the LCST, the HBP solution and silicon substrates were heated at 50 °C before deposition.

Langmuir Monolayers and Deposition. The pressure−area (Langmuir) isotherms and Langmuir−Blodgett (LB) monolayers on the silicon substrates were obtained using a KSV 2000 minithrough with water temperature control. The solutions were prepared at a concentration of 0.2 mg/mL in chloroform and then spread uniformly onto the water surface in a dropwise manner. The Langmuir monolayers were left undisturbed for 30 min to allow for equilibration and solvent evaporation. Afterward, the monolayers were compressed at a rate of 5 mm/min to the target pressure. Compression−decompression isotherms were also recorded by compressing the monolayers to the maximum pressure and then expanding to maximum trough area. The LB monolayers were transferred onto the precleaned silicon substrates via vertical dipping at a rate of 1 mm/min.

Characterization. Fourier transform infrared (FTIR) spectra were recorded using a Bruker Vertex 70 FTIR spectrophotometer operating in the 600−4500 cm^{-1} range. Samples for FTIR spectral

Scheme 1. Synthesis Pathway for Ionically Bound Thermosensitive Hyperbranched Polymers
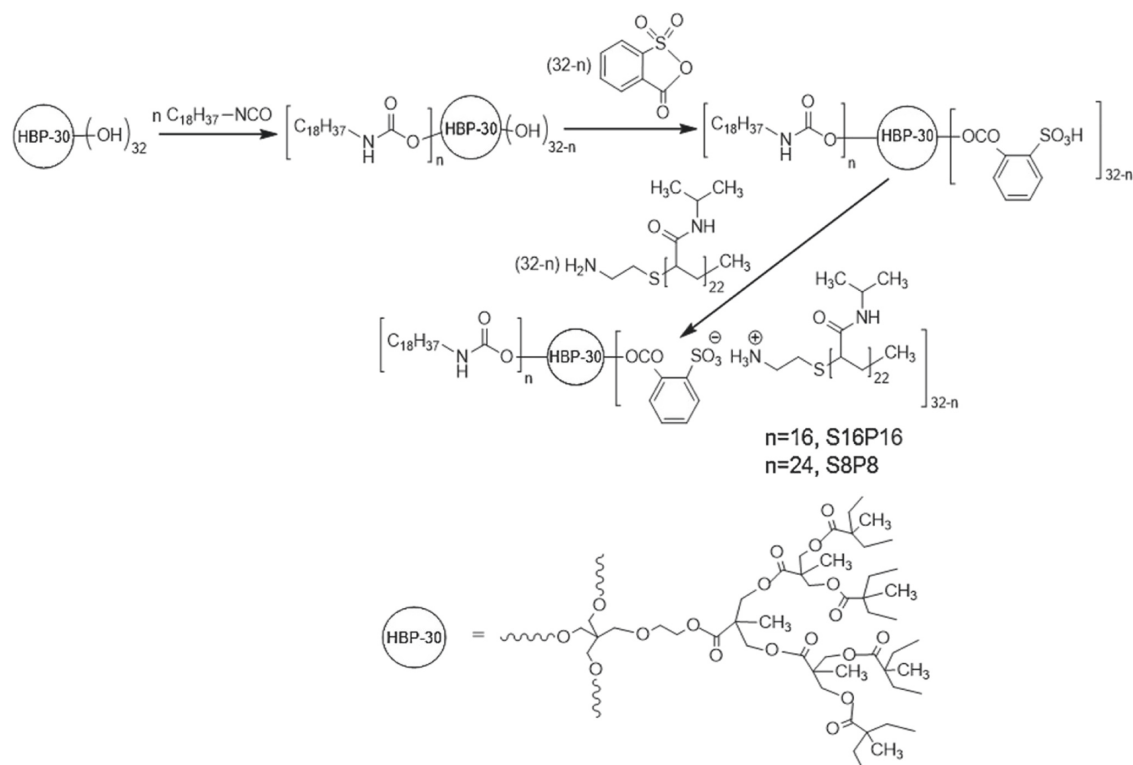
recording were prepared as pellets of the compounds mixed with KBr. Proton nuclear magnetic resonance (^{1}H NMR) spectra were recorded with a Varian VXR-400 MHz spectrometer using DMSO-d_6 (Cambridge Isotope Laboratories, Inc.). LCST behavior was investigated by observing transmittance at 500 nm with a heating/cooling rate of 0.5 °C/min (Chirascan-plus, Applied Photophysics) in the temperature range of 25−50 °C. The zeta potential and size of hyperbranched polymer assemblies in aqueous media were also measured at different temperatures using a Zetasizer Nano ZS (Malvern) with Non-Invasive Back-Scatter (NIBS) technology (HeNe gas laser operating at a wavelength of 633 nm, the scattering angle is 173°). Samples for light transmittance, zeta potential, and size measurements were all aqueous solutions at 1 mg/mL concentration.

Morphology was observed using atomic force microscopy (AFM) on an ICON microscope (Bruker) in the soft tapping mode according to the established procedure.[48] The scan rate was between 0.1 and 0.7 Hz, and the resolution was 512 × 512 or 1024 × 1024 pixels. Image analysis was carried out using Nanoscope Analysis 2.0 (Bruker). For LB monolayers, the microroughness was determined from the root-mean-square average of the height deviation taken from the 1 × 1 μm^2 areas with at least three independent locations scanned. The film thickness was also obtained using an M-2000U spectroscopic ellipsometer with WVASE32 analysis software at three incident angles of 65, 70, and 75°.[49] At least three separate locations on the sample were measured to determine the average thickness.

Surface mechanical and electrical properties of the monolayers were mapped using Peak-Force Kelvin probe force microscopy (PF-KPFM) (Bruker). We used silicon probes with a metallic back contact layer with a spring constant of 0.8 N/m and a tip radius of 5 nm (PFQNE-AL, Bruker), which are designed for PF-KPFM. Prior to each new sample measurement, tip characterization was performed. Deflection sensitivity and spring constant of the tips were determined from force−distance curves (FDCs) on a sapphire crystal. The monolayers were scanned in the PF-KPFM mode at a scan rate of 0.5 Hz and a resolution of 512 × 512 pixels. PF-KPFM measurements were conducted at a lift height of 100 nm. All images were analyzed using Nanoscope Analysis 2.0 (Bruker).

■ RESULTS AND DISCUSSION

Synthesis of Thermosensitive Hyperbranched Polymers. We synthesized amphiphilic hyperbranched polymers bearing sulfonate terminal groups ionically functionalized with thermoresponsive linear functionalized PNIPAM chains as macro-counter cations tethered to the ionized terminal groups of HPB cores with ionic interactions (Figure 1 and Figures S1−S4). The synthesized polymers belong to a special class of branched polymers with end ionized groups, which is not a traditional class of linear polyelectrolytes with a substantial portion of the constitutional units containing ionic or ionizable groups.[50] However, since the synthesized polymers are composed of branches with ionic sulfonate terminal groups as repeating units, these polymers generally belong to polyelectrolytes or ionomers depending upon molar content.

In fact, the molar contents of ionizable groups for the fourth generation of HPBs considered in this study (calculated to be around 1/2000 and 1/1200 $(g/mol)^{-1}$ for S8P8 and S16P16, respectively) approach a common border between polyelectrolytes and ionomers (between 1/500 and 1/5000 $(g/mol)^{-1}$ for polystyrene sulfonate copolymers).[51−55] In addition, because the ionic terminal groups are attached to the hyperbranched cores with multiple partially regular branches obtained via one-pot synthesis, this class of polymers is called hyperbranched polymers.[24]

Here, the hyperbranched polymers of asymmetric type (abbreviated as S8P8) were synthesized, containing 24 hydrophobic *n*-octadecylurethane arms and 8 hydrophilic PNIPAM macrocations (Figure 1a). The hyperbranched polymers of symmetric type (abbreviated as S16P16) were also produced, which contained 16 *n*-octadecylurethane and 16 PNIPAM macrocations (Figure 1b).

Scheme 1 shows a synthesis pathway of the hyperbranched polymers. The synthesis was based on partial blocking of

Table 1. Molecular Weights, Volume Ratios of *N*-Octadecylurethane Arms to PNIPAM Chains, T_g Values, and Mean DBs for the HBPs

		MW (g/mol)				
Sample	Abbreviation	Calculated	Found	V_{Oct}/V_{PNIPAM}	T_g (°C)	Mean DB (%)[34]
HBP-24Oct8[SO$_3$]$^-$ [PNIPAM]$^+$	S8P8	32,320	32,960	0.44	81.3	38.7
HBP-16Oct16[SO$_3$]$^-$ [PNIPAM]$^+$	S16P16	50,848	52,000	0.15	89.2	
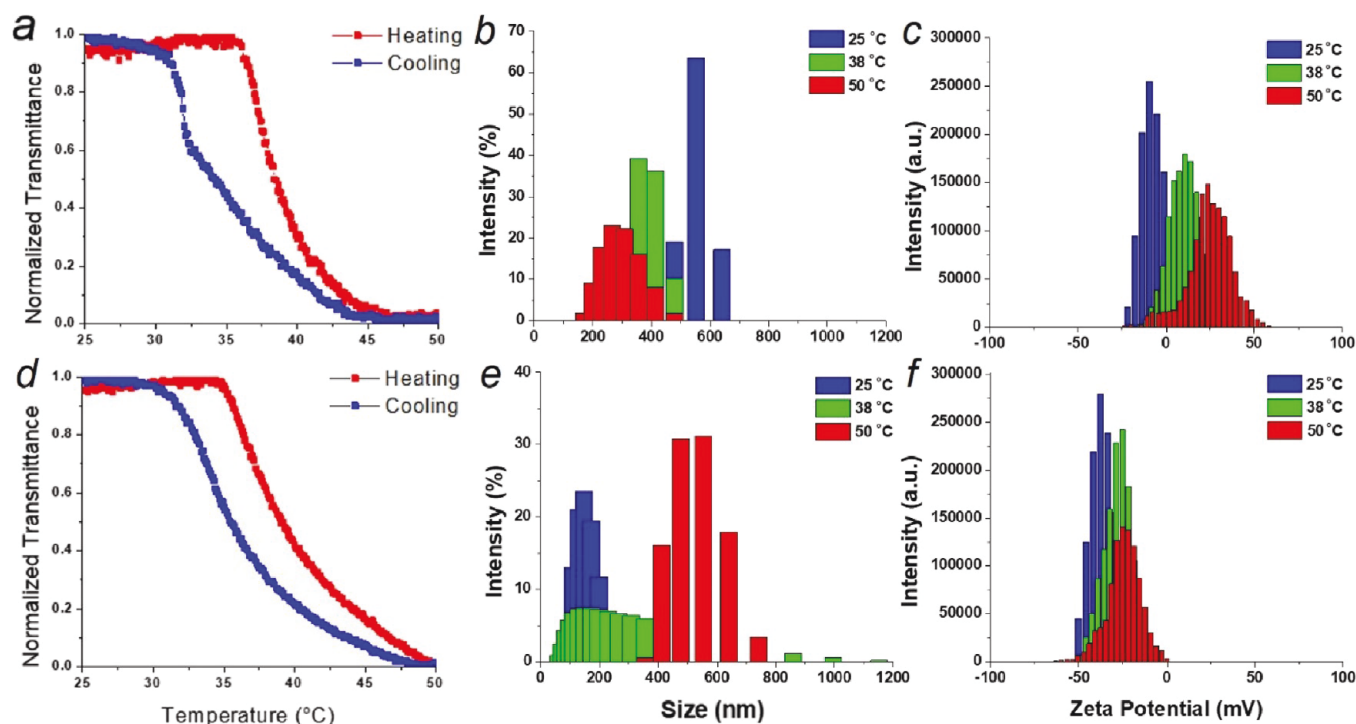
Figure 2. Transmittance (a,d), size (b,e), and zeta potential (c,f) of S8P8 (a−c) and S16P16 (d−f) HBPs vs temperature (heating and cooling rates are 0.5 °C/min for transmittance measurements).

terminal hydroxyl groups of the hyperbranched polyester polyol of pseudo-third generation by *n*-octadecylisocyanate followed by acylation of residual hydroxyl groups of the reaction product with 2-sulfobenzoic acid cyclic anhydride (see the Supporting Information for detailed information).

The chemical structures of the synthesized HBPs are confirmed by FTIR (Figure S2) and ^{1}H NMR (Figures S3−S4). The FTIR spectra of S8P8 and S16P16 show characteristic absorption bands that confirm targeted chemical compositions. The FTIR spectra exhibit the absorption bands for aliphatic fragments: ν C−H of CH$_2$ in the range of 2850−2980 cm^{-1}, ν C−H of CH$_3$ (1090−1309 cm^{-1}), δ C−H of CH$_2$, δ as C−H of CH$_3$ (1458 or 1460 cm^{-1}), and δ sy C−H of CH$_3$ (1367, 1387 cm^{-1}). The band at 1000−1090 cm^{-1} represents the ν S=O bonds of sulfonate anions, which overlap ν C−H of CH$_3$. The bands at 1650 and 1543 cm^{-1} are assigned to ν C=O amide I and δ N−H amide II, respectively, which are the characteristic bands of carbonyl groups of PNIPAM. The band at 3074 cm^{-1} represents aromatic rings (ν C−H), and the bands at 3130−3700 cm^{-1} suggest ammonium cations, amide, and urethane groups (ν N−H) (Figure S2).

The ^{1}H NMR spectra show the characteristic signals for methyl and methylene groups of the hyperbranched core, PNIPAM fragments, and *n*-octadecylurethane arms in the range of 0.74−4.30 ppm. The ^{1}H NMR spectra also exhibit the peaks of protons from tertiary carbon atoms of PNIPAM fragments (1.99/1.98, 3.85 ppm). The signals for aromatic

rings and amide groups appear in the range of 7.00−7.90 ppm, and the signal at 8.78/8.76 ppm is for ammonium cations of PNIPAM. The neutralization degree of the obtained HBPs is evidenced by both positions of protons corresponding to characteristic groups and ratios of the signal areas (Figures S3−S4).

Molecular weight (MW) values of the HBPs were determined based on the MW of the intermediate hyperbranched polysulfonic acids (from the acid−base titration technique, see the Supporting Information) and MW of PNIPAM macrocations, and the determined MW values are close to the theoretical values (Table 1). The volume fraction of *n*-octadecylurethane arms to PNIPAM chains (V_{Oct}/V_{PNIPAM}) was calculated from their molecular weights and densities. The values of V_{Oct}/V_{PNIPAM} decreased from 0.44 to 0.15 with increasing PNIPAM content. According to the results of our previous studies based on ^{13}C NMR, the starting polyester polyol HBP-OH has a degree of branching (DB) of 38.7%,[34] in good agreement with the literature data, which gives DB values of 36−43% for HBP-OH (Boltorn H40), which has a similar chemical structure to the starting HBP-OH in this study but with more terminal hydroxyl groups (64).[56] The determined DB values are valid for both intermediate hyperbranched polysulfonic acids and final HBPs (Table 1).

Thermal Behavior of Thermosensitive Hyperbranched Polymers. The differential scanning calorimetry (DSC) curves of S8P8 and S16P16 show glass transition

temperatures (T_g) of 81 and 89 °C, respectively, indicating an amorphous state without signs of crystallization (DSC methodology and curves in Figure S5). The T_g values for these compounds are significantly lower than those of regular high-molecular-weight PNIPAM materials (within 110−140 °C).[57−59] This depression is due to the low T_g of the hyperbranched polyester core with T_g values of similar branched polyester polyols reported to be within 25−40 °C.[60−62] The hyperbranched polyesters with terminal alkyl fragments obtained in our previous study have a T_g value of −30 °C and melting points of 40−60 °C, attributed to the crystalline phase formed by the alkyl component.[63] The absence of melting peaks for S8P8 and S16P16 can be related to the suppression of crystallization of the alkyl branched components by adjacent PNIPAM macrocations.[62]

In aqueous solutions, S8P8 and S16P16 showed a broad LCST transition with modest hysteresis (4−6 °C) (Figure 2a,d). This is in contrast to a sharp LCST transition of traditional linear PNIPAM homopolymers around 32 °C.[64] The PNIPAM macrocations with highly polar ammonium end groups and their mobile tethering cause broadening and LCST shift toward higher temperature in comparison with common linear PNIPAMs.[65,66]

S8P8 have a higher LCST around 36.5 °C than S16P16 around 35 °C (defined as the temperature where the transmittance decreases by 10% from the initial transmittance during heating).[67,68] This result is in contrast to those found for PNIPAM-containing copolymers where increasing hydrophobicity causes a decrease in LCST.[69,70] A possible explanation for the opposite LCST trend is that the number of ionically tethered PNIPAM macrocations for S8P8 is too small to create strong intermolecular interactions between PNIPAM, which induce a coil-to-globule transition of PNIPAM at lower temperatures despite the increased hydrophobicity. In other words, the lower density of PNIPAM terminal chains for S8P8 makes PNIPAM chain aggregation less likely to occur, increasing the overall entropy of the system through aggregation between PNIPAM chains and thus resulting in a higher LCST. A similar observation was reported for PINPAM-grafted copolymers with different graft lengths: for longer PNIPAM grafts, chain aggregation was limited due to fewer chain ends in the grafts, resulting in a greater entropy contribution and a higher LCST.[71] It was also reported that the LCST transition of end grafted PNIPAM with a low chain grafting density was very subtle due to weak attractive interactions between PNIPAM chains.[72,73]

In addition, S8P8 and S16P16 HBPs showed temperature-induced size change, reflecting the LCST transition of PNIPAM (Figure 2b,e). Interestingly, S8P8 and S16P16 HBPs exhibited an opposite trend in size change upon heating. S8P8 HBPs had an average size of 0.56 ± 0.05 μm at 25 °C and gradually decreased to 0.32 ± 0.06 and 0.29 ± 0.00 μm at 38 and 50 °C, respectively. For S16P16 HBPs, the average size was 0.31 ± 0.07 μm at 25 °C. This value is comparable to that of spherical assemblies (e.g., vesicles) formed by amphiphilic hyperbranched copolymers composed of an initial core that is the same as with S16P16.[74,75] When temperature increased to 38 °C, S16P16 HBPs showed a broad size distribution with an increased average size of 0.38 ± 0.04 μm. Further heating to 50 °C led to the size increase to 0.57 ± 0.05 μm. These results indicate that a significant molecular reorganization of S8P8 and S16P16 HBPs takes place with increasing temperature.

The zeta potential values of S8P8 and S16P16 HBPs also changed in response to temperature (Figure 2c,f). S8P8 and S16P16 HBPs had average zeta potential values of −9 ± 2 and −39 ± 2 mV, respectively, at 25 °C. The lower zeta potential for S8P8 is due to a lower density of ionic terminal groups. The zeta potential value of S16P16 is comparable to that of hyperbranched polymers bearing 50% sulfonate terminal groups reported in the literature (Figure 2f).[76] Indeed, sulfonate-terminated HBPs have shown negative zeta potentials from −60 to −20 mV, depending on the density of terminal ionic groups and the type of counter ion.[46,76] S16P16 exhibited a lower negative zeta potential than the HBPs with the same chemical structure as S16P16 but small counter ions (around −60 mV).[46] This indicates that large PNIPAM macrocations partially screen the core sulfonate anions.[33]

The zeta potential value increased from −9 to 11 mV for S8P8 and from −39 to −28 mV for S16P16 upon heating to 38 °C. The values further increased to 24 and −24 mV for S8P8 and S16P16, respectively, as temperature increased to 50 °C. This result indicates that collapsed PNIPAM macrocations above the LCST screen the sulfonate terminal groups of the core with ammonium end groups of PNIPAM macrocations being exposed to the surface of the HBP micelles and molecules. A similar change in surface charge upon heating was observed for other classes of HBPs with PNIPAM macrocations[33] and PNIPAM-polycation block copolymers.[77,78]

Assembly of Thermosensitive Hyperbranched Polymers. *Morphology of Drop-Cast Films.* First, solutions of S8P8 and S16P16 were drop-cast on silicon substrates and allowed to dry. The morphology of the dried films depended on peripheral chemical composition of the HBPs. S8P8 HBPs formed a planar network-like structure, whereas S16P16 HBPs formed vesicles with a size of 0.43 ± 0.17 μm (Figure S6). This morphological change can be explained by the increased hydrophilicity by increasing the number of PNIPAM macrocations. It has been demonstrated that hydrophilic/hydrophobic balance is critical for determining the morphology of amphiphilic block copolymers in aqueous media and increasing the volume fraction of hydrophobic blocks can lead to the morphological transition from vesicles to lamellar structures.[79−81]

Above the LCST (50 °C), S8P8 and S16P16 HBPs formed chains of spherical structures with different heights of ∼200 and ∼800 nm, respectively (Figure S7). This temperature-induced morphological transition can be understood by the increased hydrophobicity arising from the LCST transition of PNIPAM. We suggest that although PNIPAM macrocations become hydrophobic above the LCST, the sulfonate and ammonium groups of the HBPEs are capable of bonding to water molecules. Therefore, the HBPs preserve an amphiphilic character with reduced hydrophilicity even above the LCST, allowing them to self-assemble into the spherical features. In addition, it should be noted that the dimension of S8P8 assemblies was smaller than that of S16P16 assemblies as observed by DLS (Figure 2b,e and Figure S7). Such a size difference is due to the difference in the number of charged terminal groups. We suggest that the greater number of charged terminal groups of S16P16 HBPs provides peripheral hydrophilicity strong enough to stabilize the formation of the large spherical features. On the other hand, the peripheral hydrophilicity of S8P8 HBPs created by fewer charged terminal groups results in the formation of relatively small spherical morphologies (Figure S8). Similarly, a morphological

transition from spheres through vesicles to large spherical micelles was reported for linear amphiphilic block copolymers, PS-*b*-PAA, as the volume fraction of the hydrophilic PAA block decreased.[82]

To understand the role of weakly ionically tethered macrocations on the overall assembly of the HBPs, we investigated the HBP solutions with salt-added media. First, the addition of salts caused a significant increase in the sizes of S8P8 and S16P16 HBP assemblies. With 0.1 M NaCl, the average sizes of S8P8 and S16P16 assemblies at 25 °C were 1.3 ± 0.1 and 0.52± 0.05 μm, respectively, which were about twice larger than those without salts (Figure S9a,b). Upon salt addition, the zeta potential values increased from −9 to −3 mV and from −39 to −10 mV for S8P8 and S16P16 HBPs, respectively (Figure S9c,d). This increase in the zeta potential value is attributed to the screening of the charged surface of the HBPs, which leads to the presence of fewer ions in the diffuse layer and then to a lower absolute value of zeta potential. Similar reduction in zeta potential was reported for hyperbranched polyions with increasing ionic strength due to decreasing ionization degree of terminal ionic groups.[46,83] The AFM images of the drop-cast films of S8P8 and S16P16 salt-added solutions also showed the formation of large, irregular aggregates, confirming that the salt addition caused the aggregation of the HBPs facilitated by the decreased ionization degree (Figure S10). Thus, we can conclude that the presence of mobile macrocations enables control of the HBP assemblies, which is not accessible for traditional neutral polymers. Next, we consider the dynamics of terminal chain assembly with molecular dynamics simulations in the following section.

Molecular Dynamics Simulations. Figure 3 shows the time evolution of two representative S16P16 HBP molecules on a
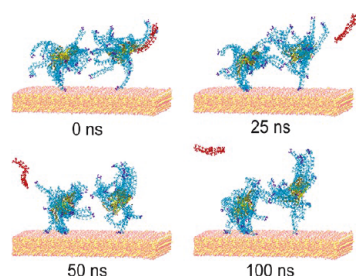

Figure 3. Molecular dynamics simulations of the assembly behavior of S16P16 HBPs on a silicon substrate that show detaching and hopping of PNIPAM macrocations (cyan) between the SO_3^- anions (orange) of the hyperbranched cores (tan). The dimethyl acetamide groups are shown in violet, and water molecules are hidden for clarity.

SiO_2 surface. We did not observe significant aggregation between the S16P16 HBPs within the simulation trajectory, primarily due to the competition between HBP−HBP and HBP−surface interactions (Figure 3 and Figure S10, Movies S1, S2). Within the first 10 ns, the terminal dimethyl acetamide groups of the PNIPAM macrocations form weak van der Waals (VDW) interactions with the hyperbranched core and macrocations of the neighboring HBPs. At the same time, the terminal dimethyl acetamide groups within the vicinity of the surface form strong interactions with the silanol surface groups (Figure 3). As a result, the surface bonding is largely dominated by VDW interactions between the silanol surface groups and the terminal dimethylacetamide groups of the PNIPAM macrocations. Overall, the HBP−surface interactions

are 2 orders of magnitude stronger than the intermolecular interactions, indicating strong surface bonding of absorbed molecules (Figure S2).

The macrocations farther away from the surface did not deposit on the surface even after 100 ns of simulation (Figure 3). The cores of the HBP molecules also do not interact favorably with the surface, mainly due to steric restrictions associated with the preferential macrocation-surface bonding. However, a hydrophobically driven clustering within macrocations is evident from the reduced radius of gyration of the molecules, which occurs due to increased intramolecular hydrogen bonding after the first 20 ns. As the radius of gyration decreased, the interaction between the neighboring HBPs was no longer noticeable after 50 ns (Figure S14).

It is critical to note that the outer PNIPAM macrocations in this study are highly mobile in contrast to traditional covalently tethered arms.[27,29] In our case, the macrocations are noncovalently attached to the core via Coulombic-controlled bonding between the terminal NH_3^+ and SO_3^- groups of terminal chains and core branches (Figure 1). Such weak bonding allows hopping between SO_3^- sites and/or completely dissociating from the core. Our simulations show that a single macrocation (out of 80 in total) was completely dissociated from the HBP core and became solvated (Figure 3). The rest of the macrocations hopped between the nearby SO_3^- sites of their respective cores, forming highly mobile coronas. In total, during the simulation cycle, about 45% of the macrocations (36 out of 80) left the original sulfonate site and did not return. The rest of the macrocations hopped between the neighboring SO_3^- with a high frequency (Figure S13). Only a small fraction of macrocations (10%) remained tethered to their original sulfonate sites for more than 80 ns (Figure S13). Thus, overall, about 90% of the PNIPAM macrocations are dynamically hopping between the SO_3^- terminal sites to balance interactions between NH_3^+ and SO_3^- ions. These detaching and hopping can lead to large mobile coronas surrounding a hydrophobic cluster, which can contribute to obtaining diverse morphological variation of HBPs under changing assembling conditions (Movie S3).

Hyperbranched Polymers at the Air−Water Interface. To further investigate the role of the weakly tethered PNIPAM macrocations, we studied their interfacial assembly behavior at the air−water interface with a strong vertical amphiphilicity-driven segregation trend caused by the interface between the water subphase and air as a poor solvent for these molecules.

Langmuir Monolayers. The pressure−area isotherms of Langmuir monolayers from S8P8 and S16P16 HBPs show the formation of stable monolayers with characteristic gas, liquid expanded and condensed phases, and solid phase, confirmed by a steady increase in surface pressure upon compression (Figure 4).[63] The isotherms for S8P8 HBPs were shifted toward a smaller surface area compared to those for S16P16 HBPs, indicating a more compact state.

This isotherm shift can be explained by stronger interactions of alkyl arms by increasing the number of alkyl arms. As the interactions of the alkyl arms increase, the alkyl arms straighten out, align parallel to each other, and arrange perpendicular to the water surface, making hyperbranched polymer molecules adapt a compact conformation and thus reducing the surface area occupied by the HBP molecule.[84] Correspondingly, the limiting mean molecular area (MMA) in a liquid phase for S8P8 HBPs (71.9 nm^2) was also smaller than that for S16P16 HBPs (90.7 nm^2) (Figures S15−S16). Moreover, increasing
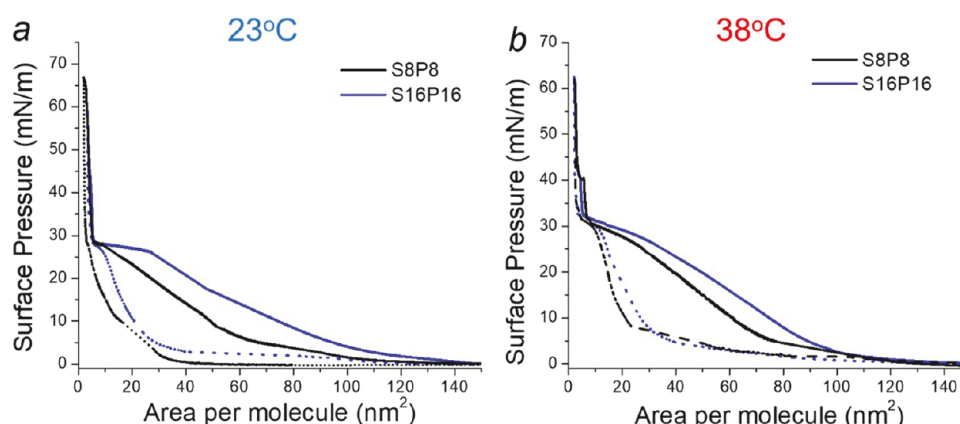
Figure 4. Langmuir pressure−area isotherms of S8P8 and S16P16 HBPs at ambient temperature (a) and 38 °C (b).

the water subphase temperature above the LCST does not change the overall character with a slightly smoother pressure increase (Figure 4 and Figures S15−S16).

LB Monolayer Morphology. The AFM images of LB monolayers show that circular domains were formed in a liquid phase (at 20 mN/m) and transformed into coalescent domain morphologies in a solid phase (at 50 mN/m) (Figures S18−S19). These morphologies are different from those of the drop-cast films, suggesting that the organization of hyperbranched polymers in a 3D environment (in aqueous media) is distinct from that in a 2D confined environment (at the air−water interface). In the aqueous media, PNIPAM macrocations are highly mobile, while the lateral compression within monolayers promotes strong segregation where attached macrocations submerged into the water subphase.

The high-resolution AFM images show that S8P8 and S16P16 HBPs formed circular domains with heights of 2−3 nm in the liquid phase for both temperatures (Figure 5). The diameter of the circular domains depends on peripheral chemical composition as well as water subphase temperature. At ambient temperature, the circular domains formed by S8P8 HBPs have an average diameter of 2.8 ± 0.8 μm and height of 3.1 ± 1.0 nm (Figure 5a). The domain diameter decreases to 0.53 ± 0.27 μm upon heating above the LCST with an average height of 2.9 ± 0.6 nm (Figure 5b). In addition, S16P16 HBPs formed circular domains with much smaller diameters. At ambient temperature, the circular domains have an average diameter of 60 ± 3 nm and height of 2.3 ± 0.3 nm, whereas circular domains at 38 °C have a larger average diameter of 110 ± 58 nm and height of 3.2 ± 0.3 nm (Figure 5c,d).

Upon compression, the morphological transition occurred where the circular domains became porous for both temperatures for S8P8 monolayers (Figure 6). The S8P8 monolayer at ambient temperature showed elevated structures connecting each other and surrounding hole-like regions. The elevated network-like structures have an average height of 6.3 ± 0.9 nm. Pillars with an average height of 17.7 ± 5.5 nm were also observed in the monolayer (Figure 6a). Above the LCST, the monolayer showed elevated but wide structures of 8.0 ± 1.2 nm height with a few towering pillars of 26.5 ± 6.6 nm height (Figure 6b). On the other hand, S16P16 monolayers in the solid phase exhibited a relatively continuous morphology. At ambient temperature, protruding islands were formed with an average height of 7.7 ± 1.3 nm (Figure 6c). Upon heating to 38 °C, the monolayer contained flat domains with pillar-like and ring-like features formed. The average heights of the flat
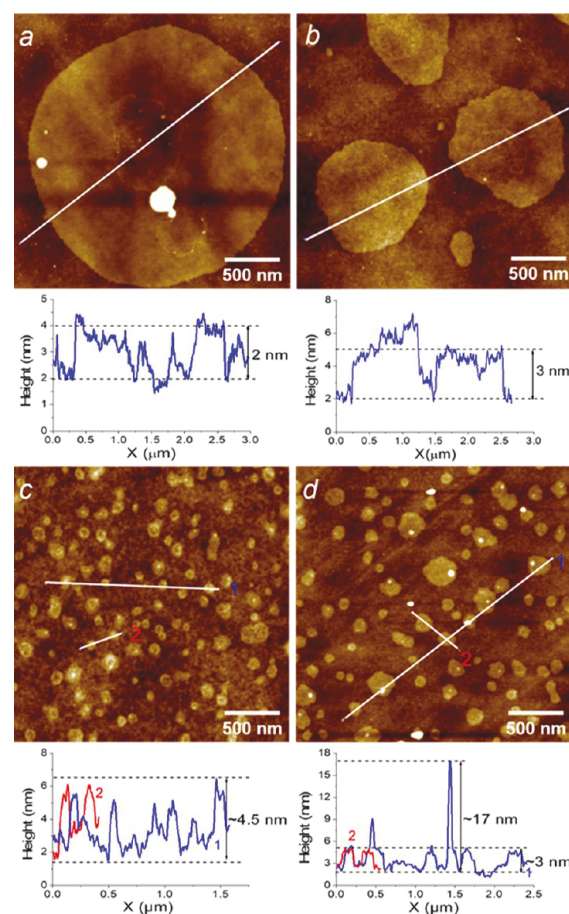

Figure 5. AFM topography images and height profiles of S8P8 (a,b) and S16P16 (c,d) monolayers at 20 mN/m and at different temperatures; ambient temperature (a,c) and 38 °C (b,d). Z scales are 10 nm for all images.

domains and elevated pillars are 2.4 ± 0.6 and 13.1 ± 3.5 nm, respectively (Figure 6d). The morphological variation depending on the peripheral composition and deposition condition can be also seen in the AFM three-dimensional images and phase images (Figures S20−S23).

Monolayer Formation. Considering that AFM provides only the surface morphology, we analyzed the data on heights and area fraction of the domains obtained from the profile analysis of AFM topography images and effective thicknesses of the monolayers measured by ellipsometry (Tables 2−3).
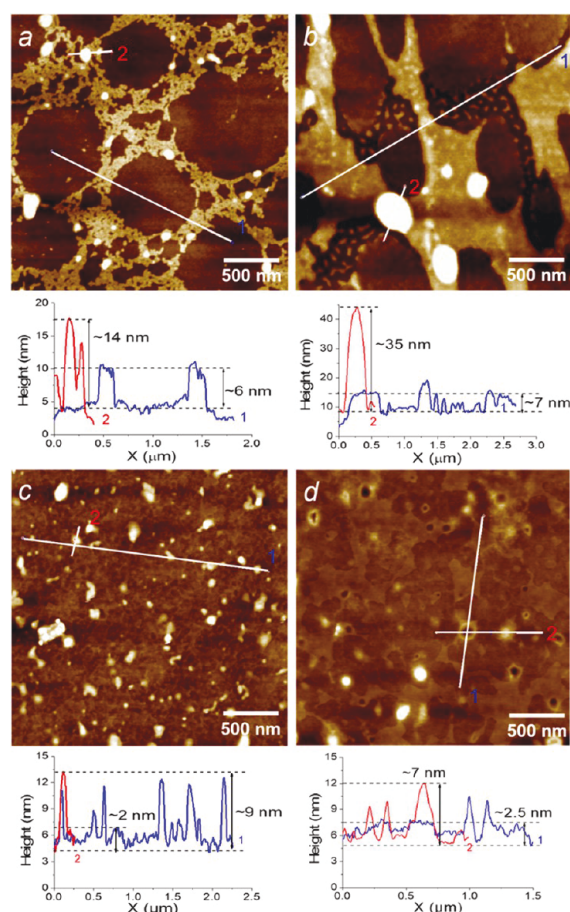
Figure 6. High-resolution AFM topography images and height profiles of S8P8 (a,b) and S16P16 (c,d) monolayers at 50 mN/m and at different temperatures; ambient temperature (a,c) and 38 °C (b,d). Z scales are 15 nm for all images.

The effective thickness of the monolayers in the liquid phase was measured to be 0.8−1.4 nm (Figure S24). The effective thickness $t_{effective}$ is calculated as $A_{domain,1}(h_{domain,1} + t_{under}) + A_{domain,2}(h_{domain,2} + t_{under}) + \cdots + A_{domain,n}(h_{domain,n} + t_{under}) + A_{under}(t_{under})$, where $A_{domain,1}$, $A_{domain,2}$, $\cdots$, $A_{domain,n}$ and A_{under} are the area fraction of n different domains and the underlying sublayer, respectively, $h_{domain,1}$, $h_{domain,2}$, $\cdots$, $h_{domain,n}$ are the heights of the domains, and t_{under} is the thickness of the underlying sublayer.[85] From this equation, the thicknesses of the underlying sublayer were calculated to be 0.1 and 0.6 nm for the S8P8 monolayers in the liquid phase at ambient temperature and 38 °C, respectively. For the S16P16 monolayers in the liquid phase, the calculated thicknesses of the underlying sublayer were 0.3−0.5 nm for both temperatures.

The analysis on the heights and effective thickness was also performed for the monolayers in the solid phase. The effective thicknesses of the S8P8 monolayers in the solid phase were measured to be 4.7 and 6.3 nm for ambient temperature and 38 °C, respectively (Figure S24). The thicknesses of the underlying sublayer were calculated to be 2.1 and 3.6 nm for ambient temperature and 38 °C, respectively, implying that the circular regions, which look like holes, are not perforated. For the S16P16 monolayers, the effective thicknesses were 3.5 and 6.3 nm, and the calculated thicknesses of the underlying sublayer were 3.0 and 5.1 nm for ambient temperature and 38 °C, respectively.

A model for the monolayer organization that fulfills the morphological observations and analysis is suggested in Figure 7. In the liquid phase, hydrophilic PNIPAM macrocations spread under water, while hydrophobic core-branch segments tend to combine together across the air−water interface to avoid unfavorable interactions with water and form compact globules that sit above PNIPAM, resulting in the formation of circular domains, known as "pancake-like" structures commonly observed for LB monolayers of amphiphilic block copolymers.[86,87] It is worthy to note that the dimension of circular domains can be controlled by adjusting the peripheral chemical composition of the hyperbranched polymers as well as temperature. First, the circular domains formed by S8P8 HBPs have a larger dimension than those by S16P16 HBPs. As the number of alkyl arms decreases, the hydrophobic interactions between them get weaken, making hyperbranched polymer molecules less closely packed. Meanwhile, increasing the number of PNIPAM macrocations also leads to greater separation between the molecules, limiting the combination of hydrophobic segments in a large domain. Thus, the domains for S16P16 HBPs with fewer alkyl arms and more PNIPAM macrocations grow smaller than those for S8P8 HBPs (Figure 7).

Above the LCST, hydrophobized PNIPAM chains preferentially absorb at the water surface. For S8P8 HBPs, as a large number of molecules combine together, the PNIAPM chains anchored at the water surface act as barriers and prevent additional aggregation of the molecules. Therefore, the domain diameter above the LCST is smaller than below the LCST. In contrast, since the domains of S16P16 HPBs consist of fewer molecules, the barrier effect of the hydrophobized PNIPAM chains seems insignificant. For S16P16 HBPs, circular domains with increased effective volume were formed above the LCST.

Upon compression to the solid phase, the hyperbranched polymer molecules are closely packed while adapting the compact conformation with alkyl arms and PNIPAM chains being vertically oriented, resulting in the formation of coalescent morphologies. At first glance, the S8P8 monolayers displayed porous morphology, whereas S16P16 HBPs formed condensed monolayers. Based on the analysis on height and

Table 2. Parameters Analyzed for Estimating Underlying Sublayer Thickness for S8P8 Monolayers

	23 °C			38 °C		
	20 mN/m	50 mN/m		20 mN/m	50 mN/m	
Domain shape	Disk	Network	Pillar	Disk	Network	Pillar
Domain height (nm)	3.1 ± 1.0	6.3 ± 0.9	17.7 ± 5.5	2.9 ± 0.6	8.0 ± 1.2	26.5 ± 6.6
Domain surface coverage (%)	25.6 ± 3.9	36.7 ± 1.5	1.4 ± 0.5	27.4 ± 2.6	20.6 ± 1.4	3.9 ± 1.1
Film thickness (nm)	0.9 ± 0.0	4.7 ± 0.1		1.4 ± 0.0	6.3 ± 0.4	
Estimated underlying sublayer thickness (nm)	0.1	2.1		0.6	3.6	

Table 3. Parameters Analyzed for Estimating Underlying Sublayer Thickness for S16P816 Monolayers

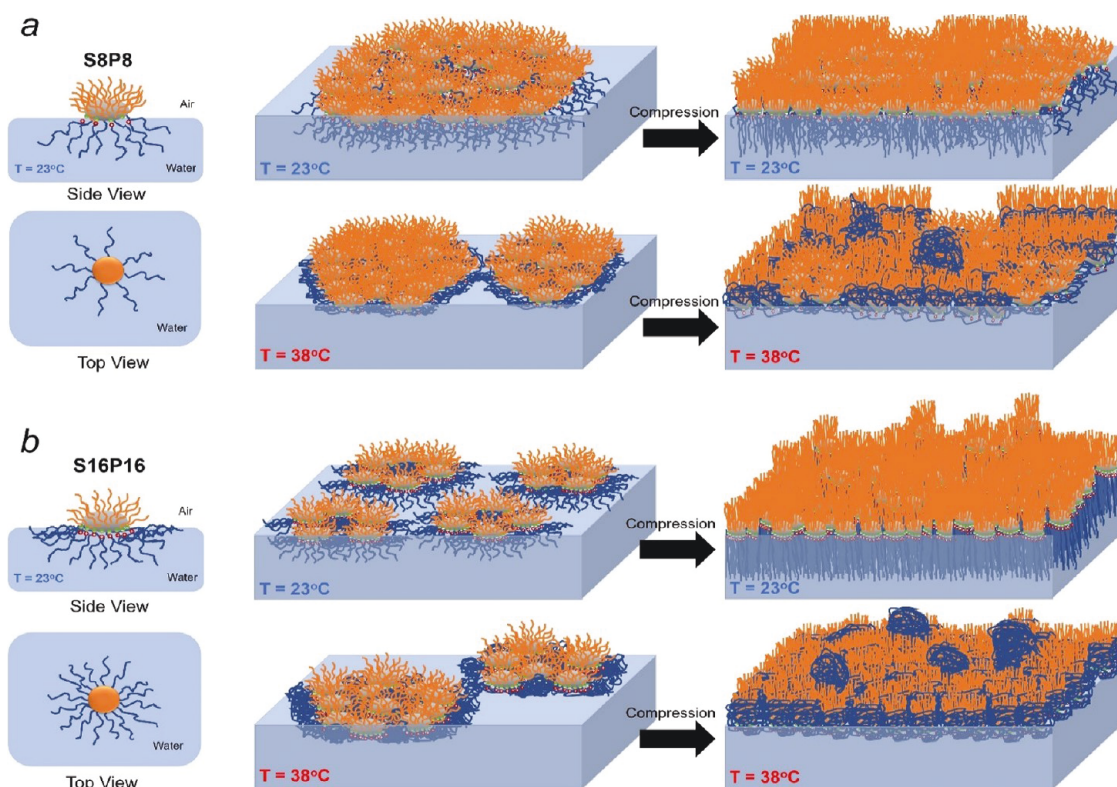|	23 °C		50 °C		
	20 mN/m	50 mN/m	20 mN/m	50 mN/m	
Domain shape	Disk	Island	Disk	Flat	Pillar
Domain height (nm)	2.3 ± 0.3	7.7 ± 1.3	3.2 ± 0.3	2.4 ± 0.6	13.1 ± 3.5
Domain surface coverage (%)	13.5 ± 1.1	7.0 ± 1.1	16.2 ± 1.4	38.8 ± 3.4	1.9 ± 0.7
Film thickness (nm)	0.8 ± 0.0	3.5 ± 0.0	0.9 ± 0.1	6.3 ± 0.1	
Estimated underlying sublayer thickness (nm)	0.5	3.0	0.3	5.1	

Figure 7. Schematic of the molecular conformations of S8P8 (a) and S16P16 (b) HBPs at the air−water interface (left); suggesting monolayer formations at different surface pressures and temperatures (right).

effective thickness, the hole-like regions are not open space. We suggest that these hole-like regions in the S8P8 monolayers are formed since part of the initial circular domains are preserved to high pressures (Figure 7a). This is supported by the fact that the thickness of the sublayer (2.1−3.6 nm) is close to the sum of the initial heights of circular domains (2−3 nm) and the thickness of the underlying sublayer in the liquid phase (0.1−0.6 nm).

The high stability of the circular domains is attributed to the branched architecture and asymmetric chemical composition of S8P8 HBPs. It has been demonstrated that branched copolymers of asymmetric chemical composition with higher content of hydrophobic arms form stable circular domains at the air−water interface, which are preserved to high pressures.[34,88] Crowding of multiple hydrophobic arms tethered to a single joint point would favor the formation of highly curved, but stable interfaces, which allow the polymer morphology buried in a circular shape territory, making the transition from spherical to cylindrical morphologies unlikely to happen.[88] For S16P16 HBPs with symmetric peripheral chemical composition, segregation of hydrophobic arms would lead to the formation of a less curved interface, making circular domains more vulnerable to pressure, which causes a

morphological transition to a continuous monolayer during compression in the S16P16 monolayers (Figure 7b).[88,89] Above the LCST, the hydrophilic-to-hydrophobic transition of terminal PNIPAM chains promotes rearrangement of the whole HBP molecules. The hydrophobic PNIPAM chains in this state are absorbed at the water surface contributing to the formation of surface morphology with additional features (Figure 7).

Surface Mechanical and Electrical Properties of Monolayers. Not only surface morphology but also surface mechanical and surface charge distribution of the monolayers can be tuned by adjusting the peripheral chemical compositions as discussed in this section. Peak-Force Kelvin probe force microscopy (PF-KPFM) was performed to map the surface properties of the HBP monolayers. First, the circular domains formed in the liquid phase showed a lower elastic modulus, adhesion, and surface potential than the interdomain region for both temperatures (Figures S25−S28). The higher elastic modulus of the interdomain region can be explained by the effect of stiff silicon substrates. The elastic modulus of silicon has been reported to be in the range of 60−240 GPa, measured by AFM.[90,91] This value is much higher than those of the components of the hyperbranched polymers.
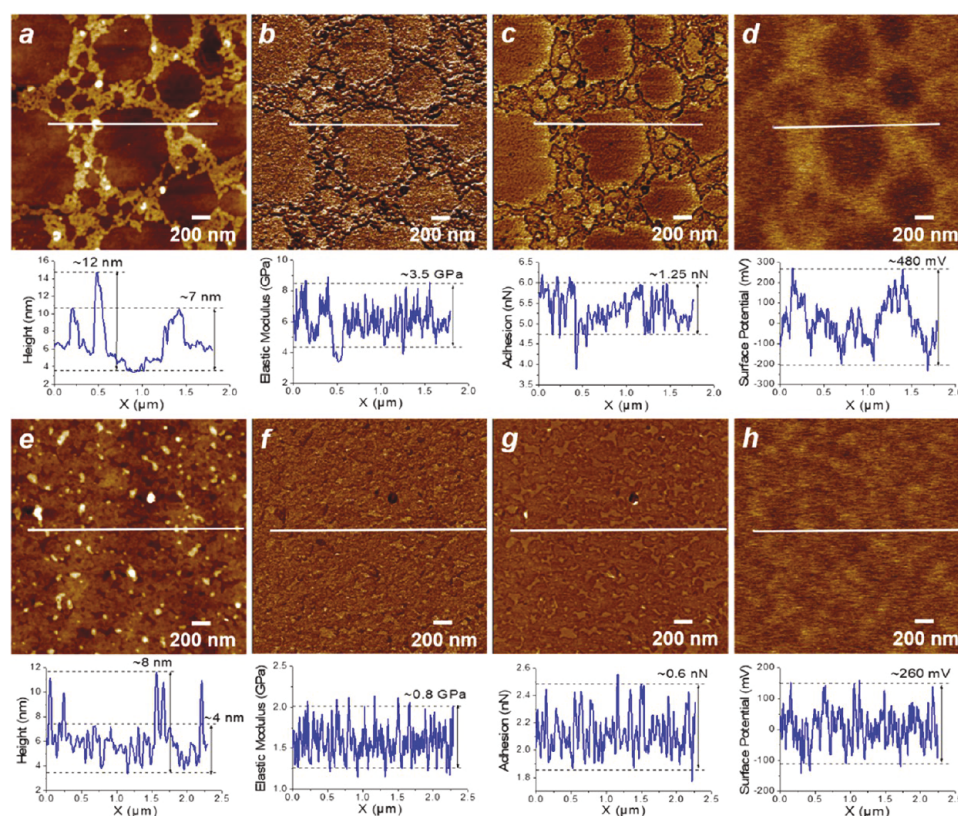
Figure 8. AFM topography (a,e), elastic modulus (b,f), adhesion (c,g), and surface potential (d,h) images and corresponding profiles of S8P8 (a–d) and S16P16 (e–h) monolayers at 50 mN/m and ambient temperature. Z scales are 15 nm for panels (a,e), 5 GPa for panel (b), 2.5 GPa for panel (f), 3 nN for panels (c,g), and 1 V for panels (d,h).

Several AFM studies have demonstrated that the estimated elastic moduli of the initial hyperbranched polyester core,[92] alkyl arms,[93,94] and PNIPAM[95] were 100−300 MPa, 1−5 GPa, and 70−100 kPa, respectively.

The circular domains showed a lower surface potential than the interdomain region although the surface potential contrasts in S16P16 monolayers were less apparent than those in S8P8 monolayers, probably owing to the existence of fewer molecules in the circular domains of S16P16 (Figures S25−S28). The lower surface potential of the domains originates from the presence of negatively charged covalently bound sulfonated terminal groups of the hyperbranched polymers. It is expected that a dipole layer was formed in the domains with negative charges residing at the substrate/monolayer interface and positive charges at the monolayer/air interface, thus resulting in the lower surface potential than that of the interdomain region. Indeed, deposition of anionic polymers causes a decrease in surface potential, whereas an increased surface potential was observed for cationic polymer domains.[96,97]

In the solid phase, the monolayers at ambient temperature showed a rather uniform modulus and adhesion distribution, supporting the suggested model in which the topmost surface of the monolayers does not consist of dissimilar components. With reorganization of HBP molecules under high compression of Langmuir monolayers, hydrophobic core-arm segments are located at the topmost surface with the beneath hydrophilic segments (Figure 8b,c and Figure S29b,c). Meanwhile, surface potential images exhibited a remarkable contrast (Figure 8d and Figure S29d). Above the LCST, the modulus and adhesion distribution of the monolayers became heterogeneous,

supporting that the topmost surface of the monolayers is composed of dissimilar components, including hydrophobized PNIPAM chains and hydrophobic core segments as suggested in Figure 7 (see Figure 9b,c and Figure S30b,c). A significant contrast in surface potential was observed for all states (Figure 9d and Figure S30d). The surface potential contrasts in the solid phase arise from the difference in net dipole distribution. Although the topmost layer of all monolayers in the solid phase is mostly composed of alkyl tails, the alkyl arms are vertically aligned or inclined to some extent associated with the presence of adjacent alkyl arms or PNIPAM chains as suggested in the monolayer formation model (Figure 7). The difference in the orientation of alkyl arms between surface features causes the distinction in net dipole moment, resulting in the surface potential contrast. It was reported that the molecule orientation affected the true dipole moment, and thus, experimentally measured surface potential of the molecule-covered region differed from theoretical results calculated for vertically aligned molecules.[98]

To further elucidate the origin of surface potential contrast, we performed PK-KPFM to compare the surface potential between the SiO_2-exposed region and monolayer region. We scratched the monolayer films with a sharp needle to expose the silicon substrate covered with a SiO_2 layer of ∼2 nm. For all monolayers, the surface potential of the bare SiO_2-exposed region was higher than that of the HBP monolayer regions (Figure 10 and Figure S31).

This result suggests that the surface potential contrasts in the monolayers are attributed to the net dipole distribution caused by the difference in molecular composition and orientation, rather than the substrate effect associated with the thickness
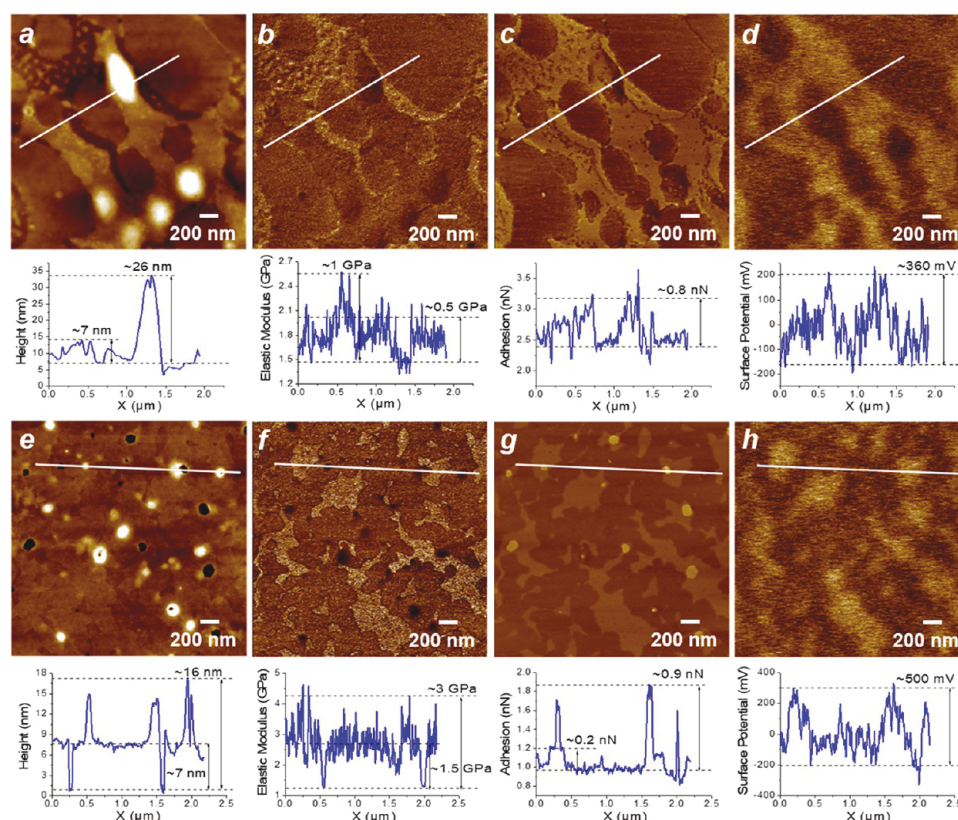
Figure 9. AFM topography (a,e), elastic modulus (b,f), adhesion (c,g), and surface potential (d,h) images and corresponding profiles of S8P8 (a–d) and S16P16 (e–h) monolayers at 50 mN/m and 38 °C. Z scales are 15 nm for panel (a), 30 nm for panel (e), 2.5 GPa for panel (b), 5 GPa for panel (f), 3 nN for panels (c,g), and 1 V for panels (d,h).
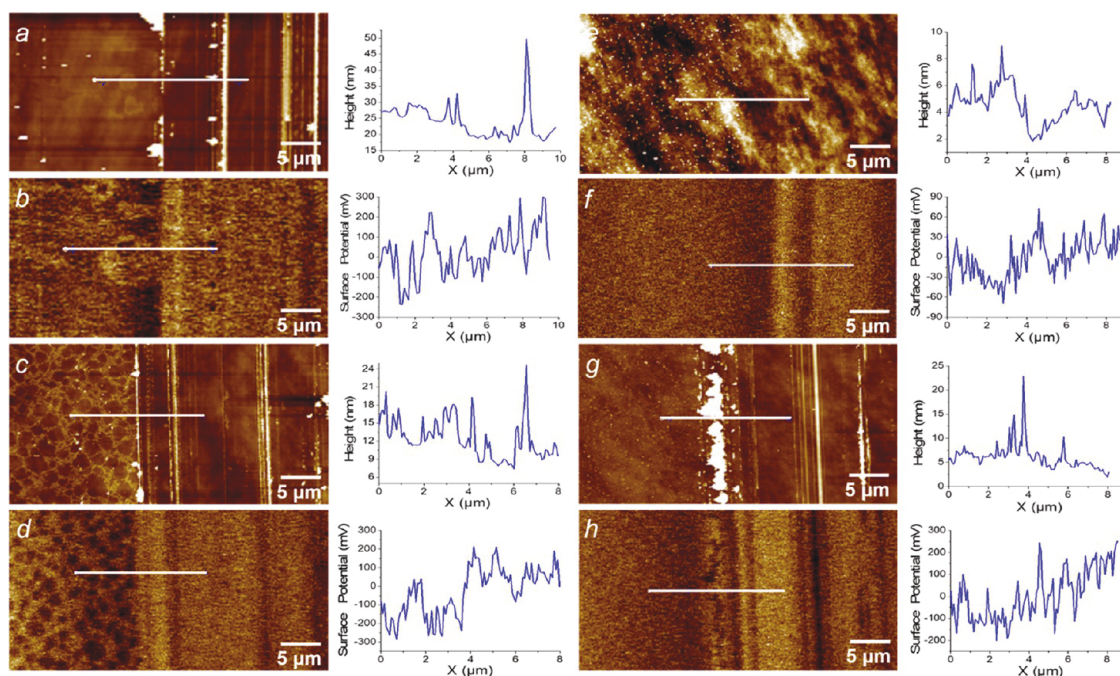

Figure 10. AFM topography (a,c,e,g) and surface potential (b,d,f,h) images and corresponding profiles of S8P8 (a–d) and S16P16 (e–h) monolayers with the SiO$_2$-exposed region at ambient temperature at different surface pressures: 20 (a,b,e,f) and 50 mN/m (c,d,g,h). Z scales are 50 nm for panels (a,g), 30 nm for panel (c), 7 nm for panel (e), 1 V for panels (b,d,h), and 0.3 V for panel (f).

difference between the domains. As known, the surface potential difference between the monolayers and SiO$_2$-exposed

region is described by $V_{monolayer} - V_{SiO_2} = \frac{\mu_{monolayer}}{A_{monolayer}\varepsilon_{monolayer}\varepsilon_0}$, where $V_{monolayer}$ and V_{SiO_2} are the surface potentials of the

monolayer and SiO$_2$-exposed regions, respectively, $\mu_{monolayer}$ is the net dipole moment of the monolayer directed normally to the substrate surface, $A_{monolayer}$ is the area occupied by each molecule, and $\varepsilon_{monolayer}$ and ε_0 are the permittivities of the monolayer and free space, respectively.[98] This relationship suggests that the surface potential contrasts in the monolayers can be governed by the dipole moments formed by the presence of negatively charged sulfonate groups residing at the substrate/monolayer interface and affected by molecular orientations.

CONCLUSIONS

In conclusion, we report the assembly behavior of novel amphiphilic hyperbranched polymers weakly, ionically bound with PNIPAM macrocations of variable contents. Terminal, mobile PNIPAM chains provide HBPs with a dynamic response due to not only their thermoresponsive behavior but also labile ionic bonding, which is inaccessible to traditional covalently tethered polymer arms. Indeed, the hyperbranched polymers with PNIPAM macrocations showed a morphological transition under changing temperature and ionic strength. Molecular dynamics simulation also probes the dynamic nature of PNIPAM macrocations with about 90% of the PNIPAM macrocations hopping between terminal sulfonate groups.

In addition, the HBPs at the air−water interface underwent amphiphilicity-driven vertical segregation where PNIPAM macrocations were confined in the water subphase. Such segregation resulted in the formation of HBP monolayers with various distinct surface morphologies. Overall, circular domains were formed at modest compression and transformed into condensed morphologies at high compression. The surface morphology strongly depends on peripheral chemical composition since the variation of peripheral composition changes the molecular conformation, organization, and resulting morphology. S8P8 HBPs with 24 alkyl arms and 8 PNIPAM macrocations take a more compact molecular conformation and organize into a more curved but stable interface than S16P16 HBPs with 16 alkyl arms and 16 macrocations. Therefore, S8P8 HBPs formed much larger circular domains, and these domains were partially preserved even at very high pressure. Increasing the temperature above the LCST also causes a morphological transition to more complex morphologies since hydrophobized PNIPAM chains are involved in surface morphology formation. Moreover, the surface mechanical and electrical responses were governed by changing the assembling condition. In particular, the presence of negatively charged sulfonate groups at the substrate/monolayer interface induces the formation of a dipole layer, promoting surface potential contrast caused by the difference in dipole distribution between domains. Changes in the assembling condition cause rearrangement of HBP molecules facilitated by LCST behavior of PNIPAM macrocations, which makes them hydrophobic above the LCST, resulting in redistribution of net dipole moments and thus surface potential contrast as measured with KPFM. Consequently, the hyper-branched polymers with weakly bound terminal PNIPAM macrocations provide opportunities for concurrent control over morphology and mechanical and electrical responses by adjusting peripheral composition or changing assembling conditions, which are difficult to achieve using traditional polymers with covalently bound arms. The tunable morphology and properties of HBPs hold promising potential for a wide range of applications where responsive nanostructures are required.

ASSOCIATED CONTENT

Supporting Information

The Supporting Information is available free of charge at https://pubs.acs.org/doi/10.1021/acs.langmuir.0c03487.

Synthesis of hyperbranched polymers, NMR, FTIR, and DSC data, AFM images, molecular dynamics simulations, and Langmuir isotherms (PDF)

Top-view of MD scenario of five S16P16 molecules on a SiO2 surface; significant aggregation between the S16P16 HBPs within the simulation trajectory, primarily due to the competition between HBP−HBP interactions (MP4)

Side-view of MD scenario of five S16P16 molecules on a SiO2 surface (MP4)

MD simulation of dectaching and hopping of a PNIPAM macrocation (MP4)

AUTHOR INFORMATION

Corresponding Author

Vladimir V. Tsukruk − *School of Materials Science and Engineering, Georgia Institute of Technology, Atlanta, Georgia 30332, United States;* orcid.org/0000-0001-5489-0967; Email: vladimir@mse. gatech.edu

Authors

Hansol Lee − *School of Materials Science and Engineering, Georgia Institute of Technology, Atlanta, Georgia 30332, United States*

Alexandr Stryutsky − *Institute of Macromolecular Chemistry of the National Academy of Sciences of Ukraine, Kyiv 02160, Ukraine*

Akhlak-Ul Mahmood − *Department of Materials Science and Engineering, North Carolina State University, Raleigh, North Carolina 27695-7907, United States*

Abhishek Singh − *Department of Materials Science and Engineering, North Carolina State University, Raleigh, North Carolina 27695-7907, United States*

Valery V. Shevchenko − *Institute of Macromolecular Chemistry of the National Academy of Sciences of Ukraine, Kyiv 02160, Ukraine*

Yaroslava G. Yingling − *Department of Materials Science and Engineering, North Carolina State University, Raleigh, North Carolina 27695-7907, United States*

Complete contact information is available at:
https://pubs.acs.org/10.1021/acs.langmuir.0c03487

Notes

The authors declare no competing financial interest.

REFERENCES

(1) Dobrynin, A.; Rubinstein, M. Theory of Polyelectrolytes in Solutions and at Surfaces. *Prog. Polym. Sci.* **2005**, *30*, 1049−1118.

(2) Zhulina, E. B.; Borisov, O. V. Theory of Morphological Transitions in Weakly Dissociating Diblock Polyelectrolyte Micelles. *Macromolecules* **2005**, *38*, 6726–6741.

(3) Soo, P. L.; Eisenberg, A. Preparation of block copolymer vesicles in solution. *J. Polym. Sci., Part B: Polym. Phys.* **2004**, *42*, 923–938.

(4) Hales, K.; Pochan, D. J. Using polyelectrolyte block copolymers to tune nanostructure assembly. *Curr. Opin. Colloid Interface Sci.* **2006**, *11*, 330–336.

(5) Cohen Stuart, M. A.; Hofs, B.; Voets, I. K.; de Keizer, A. Assembly of polyelectrolyte-containing block copolymers in aqueous media. *Curr. Opin. Colloid Interface Sci.* **2005**, *10*, 30–36.

(6) Borisov, O. V.; Zhulina, E. B. Reentrant Morphological Transitions in Copolymer Micelles with pH-Sensitive Corona. *Langmuir* **2005**, *21*, 3229–3231.

(7) Li, N. K.; Fuss, W. H.; Tang, L.; Gu, R.; Chillkoti, A.; Zauscher, S.; Yingling, Y. G. Prediction of solvent-induced morphological changes of polyelectrolyte deblock copolymer micelles. *Soft Matter* **2015**, *11*, 8235–8245.

(8) Sing, C. E.; Zwanikken, J. W.; de La Cruz, M. O. Electrostatic Control of Block Copolymer Morphology. *Nat. Mater.* **2014**, *13*, 694–698.

(9) Wang, X.; Hong, K.; Baskaran, D.; Goswami, M.; Sumpter, B.; Mays, J. Asymmetrical Self-Assembly from Fluorinated and Sulfonated Block Copolymers in Aqueous Media. *Soft Matter* **2011**, *7*, 7960–7964.

(10) Wang, X.; Goswami, M.; Kumar, R.; Sumpter, B. G.; Mays, J. Morphologies of Block Copolymers Composed of Charged and Neutral Blocks. *Soft Matter* **2012**, *8*, 3036–3052.

(11) Uhlík, F.; Košovan, P.; Zhulina, E. B.; Borisov, O. V. Charge-Controlled Nano-Structuring in Partially Collapsed Star-Shaped Macromolecules. *Soft Matter* **2016**, *12*, 4846–4852.

(12) Liu, H.; Li, C.; Liu, H.; Liu, S. pH-Responsive Supramolecular Self-Assembly of Well-Defined Zwitterionic ABC Miktoarm Star Terpolymers. *Langmuir* **2009**, *25*, 4724–4734.

(13) Zhai, C.; Zhou, H.; Gao, T.; Zhao, L.; Lin, S. Electrostatically Tuned Microdomain Morphology and Phase-Dependent Ion Transport Anisotropy in Single-Ion Conducting Block Copolyelectrolytes. *Macromolecules* **2018**, *51*, 4471–4483.

(14) Chopade, S. A.; Au, J. G.; Li, Z.; Schmidt, P. W.; Hillmyer, M. A.; Lodge, T. P. Robust Polymer Electrolyte Membranes with High Ambient-Temperature Lithium-Ion Conductivity via Polymerization-Induced Microphase Separation. *ACS Appl. Mater. Interfaces* **2017**, *9*, 14561–14565.

(15) Xu, Y.; Borisov, O. V.; Ballauff, M.; Müller, A. H. E. Manipulating the Morphologies of Cylindrical Polyelectrolyte Brushes by Forming Interpolyelectrolyte Complexes with Oppositely Charged Linear Polyelectrolytes: an AFM Study. *Langmuir* **2010**, *26*, 6919–6926.

(16) Larin, S. V.; Pergushov, D. V.; Xu, Y.; Darinskii, A. A.; Zezin, A. B.; Müller, A. H. E.; Borisov, O. V. Nano-Patterned Structures in Cylindrical Polyelectrolyte Brushes Assembled with Oppositely Charged Polyions. *Soft Matter* **2009**, *5*, 4938–4943.

(17) Furukawa, T.; Ishizu, K. Synthesis and Viscoelastic Behavior of Multiarm Star Polyelectrolytes. *Macromolecules* **2005**, *38*, 2911–2917.

(18) Xu, W.; Ledin, P. A.; Plamper, F. A.; Synatschke, C. V.; Müller, A. H. E.; Tsukruk, V. V. Multiresponsive Microcapsules Based on Multilayer Assembly of Star Polyelectrolytes. *Macromolecules* **2014**, *47*, 7858–7868.

(19) Bayoudh, S.; Laschewsky, A.; Wischerhoff, E. Amphiphilic hyperbranched polyelectrolytes: a new type of polysoap. *Colloid Polym. Sci.* **1999**, *277*, 519–527.

(20) Pu, K. Y.; Li, K.; Shi, J.; Liu, B. Fluorescent Single-Molecular Core–Shell Nanospheres of Hyperbranched Conjugated Polyelectrolyte for Live-Cell Imaging. *Chem. Mater.* **2009**, *21*, 3816–3822.

(21) Khanna, K.; Varshney, S.; Kakkar, A. Miktoarm Star Polymers: Advances in Synthesis, Self-Assembly, and Applications. *Polym. Chem.* **2010**, *1*, 1171–1185.

(22) Inoue, K. Functional Dendrimers, Hyperbranched and Star Polymers. *Prog. Polym. Sci.* **2000**, *25*, 453–571.

(23) Peleshanko, S.; Tsukruk, V. V. The Architectures and Surface Behavior of Highly Branched Molecules. *Prog. Polym. Sci.* **2008**, *33*, 523–580.

(24) Xu, W.; Ledin, P. A.; Shevchenko, V. V.; Tsukruk, V. V. Architecture, Assembly, and Emerging Applications of Branched Functional Polyelectrolytes and Poly(ionic liquid)s. *ACS Appl. Mater. Interfaces* **2015**, *7*, 12570–12596.

(25) Iatridi, Z.; Tsitsilianis, C. Water-Soluble Stimuli Responsive Star-Shaped Segmented Macromolecules. *Polymer* **2011**, *3*, 1911–1933.

(26) Xu, W.; Choi, I.; Plamper, F. A.; Synatschke, C. V.; Müller, A. H. E.; Melnichenko, Y. B.; Tsukruk, V. V. Thermo-Induced Limited Aggregation of Responsive Star Polyelectrolytes. *Macromolecules* **2014**, *47*, 2112–2121.

(27) Xu, W.; Ledin, P. A.; Iatridi, Z.; Tsitsilianis, C.; Tsukruk, V. V. Multiresponsive Star-Graft Quarterpolymer Monolayers. *Macromolecules* **2015**, *48*, 3344–3353.

(28) Choi, I.; Malak, S. T.; Xu, W.; Heller, W. T.; Tsitsilianis, C.; Tsukruk, V. V. Multicompartmental Microcapsules from Star Copolymer Micelles. *Macromolecules* **2013**, *46*, 1425–1436.

(29) Erwin, A. J.; Korolovych, V. F.; Iatridi, Z.; Tsitsilianis, C.; Ankner, J. F.; Tsukruk, V. V. Tunable Compartmentalized Morphologies of Multilayered Dual Responsive Star Block Poly-ampholytes. *Macromolecules* **2018**, *51*, 4800–4812.

(30) Iatridi, Z.; Tsitsilianis, C. pH Responsive Self Assemblies from an An-Core-(B-b-C)n Heteroarm Star Block Terpolymer Bearing Oppositely Charged Segments. *Chem. Commun.* **2011**, *47*, 5560–5562.

(31) Pispas, S.; Floudas, G.; Pakula, T.; Lieser, G.; Sakellariou, S.; Hadjichristidis, N. Miktoarm Block Copolymer Formation via Ionic Interactions. *Macromolecules* **2003**, *36*, 759–763.

(32) Hernandez-Ainsa, S.; Fedeli, E.; Barbera, J.; Marcos, M.; Sierra, T.; Serrano, J. L. Self-Assembly Modulation in Ionic PAMAM Derivatives. *Soft Matter* **2014**, *10*, 281–289.

(33) Korolovych, V. F.; Erwin, A.; Stryutsky, A.; Lee, H.; Heller, W. T.; Shevchenko, V. V.; Bulavin, L. A.; Tsukruk, V. V. Thermally Responsive Hyperbranched Poly(ionic liquid)s: Assembly and Phase Transformations. *Macromolecules* **2018**, *51*, 4923–4937.

(34) Lee, H.; Stryutsky, A. V.; Korolovych, V. F.; Mikan, E.; Shevchenko, V. V.; Tsukruk, V. V. Transformations of Thermosensitive Hyperbranched Poly(ionic liquid)s Monolayers. *Langmuir* **2019**, *35*, 11809–11820.

(35) Jo, Y. M.; Park, C. W.; Jung, B.; Yang, H.-M.; Kim, J.-D. Size and Morphology Control of Aggregates from Supramolecular Graft Copolymers Stabilized by Ionic Interaction. *Macromol. Chem. Phys.* **2010**, *211*, 2434–2442.

(36) Schwarz, B.; Schönhoff, M. Surface Potential Driven Swelling of Polyelectrolyte Multilayers. *Langmuir* **2002**, *18*, 2964–2966.

(37) Miller, M. D.; Bruening, M. L. Correlation of the Swelling and Permeability of Polyelectrolyte Multilayer Films. *Chem. Mater.* **2005**, *17*, 5375–5381.

(38) Tagliazucchi, M. E.; Calvo, E. J. Surface charge effects on the redox switching of LbL self-assembled redox polyelectrolyte multi-layers. *J. Electroanal. Chem.* **2007**, *599*, 249–259.

(39) Beneselfelt, T.; Pattersson, T.; Wagberg, L. Influence of Surface Charge Density and Morphology on the Formation of Polyelectrolyte Multilayers on Smooth Charged Cellulose Surfaces. *Langmuir* **2017**, *33*, 968–979.

(40) Tagliazucchi, M.; Calvo, E. J. Charge Transport in Redox Polyelectrolyte Multilayer Films: The Dramatic Effects of Outmost Layer and Solution Ionic Strength. *Chem. Phys. Chem.* **2010**, *11*, 2957–2968.

(41) Zhu, Y.; Yao, C.; Ren, J.; Liu, C.; Ge, L. Graphene improved electrochemical property in self-healing multilayer polyelectrolyte film. *Colloids Surf., A* **2015**, *465*, 26–31.

(42) Calvo, E. J.; Flexer, V.; Tagliazucchi, M.; Scodeller, P. Effects of the nature and charge of the topmost layer in layer by layer self assembled amperometric enzyme electrodes. *Phys. Chem. Chem. Phys.* **2010**, *12*, 10033–10039.

(43) Zhang, F.; Wu, Q.; Chen, Z.-C.; Li, X.; Jiang, X.-M.; Lin, X.-F. Bioactive Galactose-Branched Polyelectrolyte Multilayers and Microcapsules: Self-Assembly, Characterization, and Biospecific Lectin Adsorption. *Langmuir* **2006**, *22*, 8458−8464.

(44) Mergel, O.; Kühn, P. T.; Schneider, S.; Simon, U.; Plamper, F. A. Influence of Polymer Architecture on the Electrochemical Deposition of Polyelectrolytes. *Electrochim. Acta* **2017**, *232*, 98−105.

(45) Hofle, G.; Steglich, W.; Vorbrüggen, H. 4-Dialkylaminopyridines as Highly Active Acylation Catalysts. *Angew. Chem., Int. Ed.* **1978**, *17*, 569−583.

(46) Korolovych, V. F.; Ledin, P. A.; Stryutsky, A.; Shevchenko, V. V.; Sobko, O.; Xu, W.; Bulavin, L. A.; Tsukruk, V. V. Assembly of Amphiphilic Hyperbranched Polymeric Ionic Liquids in Aqueous Media at Different pH and Ionic Strength. *Macromolecules* **2016**, *49*, 8697−8710.

(47) Dionzou, M.; Morère, A.; Roux, C.; Lonetti, B.; Marty, J.-D.; Mingotaud, C.; Joseph, P.; Goudounèche, D.; Payré, B.; Léonetti, M.; Mingotaud, A.-F. Comparison of methods for the fabrication and the characterization of polymer self-assemblies: what are the important parameters? *Soft Matter* **2016**, *12*, 2166−2176.

(48) McConney, M. E.; Singamaneni, S.; Tsukruk, V. V. Probing soft matter with the atomic force microscopies: Imaging and force spectroscopy. *Polym. Rev.* **2010**, *50*, 235−286.

(49) Choi, I.; Suntivich, R.; Plamper, F. A.; Synatschke, C. V.; Müller, A. H. E.; Tsukruk, V. V. pH-Controlled Exponential and Linear Growing Modes of Layer-by-Layer Assemblies of Star Polyelectrolytes. *J. Am. Chem. Soc.* **2011**, *133*, 9592−9606.

(50) Hess, M.; Jones, R. G.; Kahovec, J.; Kitayama, T.; Kratochvil, P.; Kubisa, P.; Mormann, W.; Stepto, R. F. T.; Tabak, D.; Vohlidal, J.; Wilks, E. S. Terminology of Polymers Containing Ionizable or Ionic Groups and of Polymers Containing Ions. *Pure Appl. Chem.* **2006**, *78*, 2067−2074.

(51) Ting, J. M.; Wu, H.; Herzog-Arbeitman, A.; Srivastava, S.; Tirrell, M. V. Synthesis and Assembly of Designer Styrenic Diblock Polyelectrolytes. *ACS Macro Lett.* **2018**, *7*, 726−733.

(52) Fehér, B.; Zhu, K.; Nyström, B.; Varga, I.; Pedersen, J. S. Effect of Temperature and Ionic Strength on Micellar Aggregates of Oppositely Charged Thermoresponsive Block Copolymer Polyelectrolytes. *Langmuir* **2019**, *35*, 13614−13623.

(53) Bodycomb, J.; Hara, M. Light Scattering Study of Ionomers in Solution. 5. CONTIN Analysis of Dynamic Scattering Data from Sulfonated Polystyrene Ionomer in a Polar Solvent (Dimethylformamide). *Macromolecules* **1995**, *28*, 8190−8197.

(54) Qiao, X.; Weiss, R. A. Nonlinear Rheology of Lightly Sulfonated Polystyrene Ionomers. *Macromolecules* **2013**, *46*, 2417−2424.

(55) Huang, C.; Chen, Q.; Weiss, R. A. Rheological Behavior of Partially Neutralized Oligomeric Sulfonated Polystyrene Ionomers. *Macromolecules* **2017**, *50*, 424−431.

(56) Žagar, E.; Žigon, M. Characterization of a Commercial Hyperbranched Aliphatic Polyester Based on 2,2-Bis(methylol)-propionic Acid. *Macromolecules* **2002**, *35*, 9913−9925.

(57) Biswas, C. S.; Patel, V. K.; Vishwakarma, N. K.; Tiwari, V. K.; Maiti, B.; Maiti, P.; Kamigaito, M.; Okamoto, Y.; Ray, B. Effects of Tacticity and Molecular Weight of Poly(*N*-isopropylacrylamide) on Its Glass Transition Temperature. *Macromolecules* **2011**, *44*, 5822−5824.

(58) Makharza, S.; Auisa, J.; Sharkh, A. S.; Ghabboun, J.; Faroun, M.; Dweik, H.; Sultan, W.; Sowwan, M. Structural and thermal analysis of copper-doped poly(n-isopropylacrylamide) films. *Int. J. Polym. Anal. Char.* **2010**, *15*, 254−265.

(59) Ito, M.; Ishizone, T. Living anionic polymerization of *N*-methoxymethyl-*N*-isopropylacrylamide: Synthesis of well-defined poly(*N*-isopropylacrylamide) having various stereoregularity. *J. Polym. Sci., Part A: Polym. Chem.* **2006**, *44*, 4832−4845.

(60) Shi, Z.; Zhou, Y.; Yan, D. Facile fabrication of pH-responsive and size-controllable polymer vesicles from a commercially available hyperbranched polyester. *Macromol. Rapid Commun.* **2008**, *29*, 412−418.

(61) Žagar, E.; Huskič, M.; Grdadolnik, J.; Žigon, M.; Zupančič-Valant, A. Effect of annealing on the rheological and thermal properties of aliphatic hyperbranched polyester based on 2,2-bis(methylol)propionic acid. *Macromolecules* **2005**, *38*, 3933−3942.

(62) Dumitrascu, A.; Sarkar, A.; Chai, J.; Zhang, T.; Bubeck, R. A.; Howell, B. A.; Smith, P. B. Thermal properties of hyperbranched polyesters. *J. Therm. Anal. Calorim.* **2018**, *131*, 273−280.

(63) Zhai, X.; Peleshanko, S.; Klimenko, N. S.; Genson, K. L.; Vaknin, D.; Vortman, M. Y.; Shevchenko, V. V.; Tsukruk, V. V. Amphiphilic dendritic molecules: hyperbranched polyesters with alkyl-terminated branches. *Macromolecules* **2003**, *36*, 3101−3110.

(64) Halperin, A.; Kröger, M.; Winnik, F. M. Poly(N-isopropylacrylamide) phase diagrams: Fifty years of research. *Angew. Chem., Int. Ed.* **2015**, *54*, 15342−15367.

(65) Lapworth, J. W.; Hatton, P. V.; Rimmer, S. Thermally responsive gels formed from highly branched poly(N-isopropyl acrylamide)s with either carboxylic acid or trihistidine end groups. *RCS Adv.* **2013**, *3*, 18107−18114.

(66) Rimmer, S.; Carter, S.; Rutkaite, R.; Haycock, J. W.; Swanson, L. Highly branched poly-(N-isopropylacrylamide)s with arginine-glycine-aspartic acid (RGD)- or COOH-chain ends that form submicron stimulus-responsive particles above the critical solution temperature. *Soft Matter* **2007**, *3*, 971−973.

(67) Wang, L.; Wu, Y.; Men, Y.; Shen, J.; Liu, Z. Thermal-sensitive Starch-g-PNIPAM prepared by Cu(0) catalyzed SET-LRP at molecular level. *RSC Adv.* **2015**, *5*, 70758−70765.

(68) Denmark, D. J.; Bradley, J.; Mukherjee, D.; Alonso, J.; Shakespeare, S.; Bernal, N.; Phan, M. H.; Srikanth, H.; Witanachchi, S.; Mukherjee, P. Remote triggering of thermoresponsive PNIPAM by iron oxide nanoparticles. *RCS Adv.* **2016**, *6*, 5641−5652.

(69) Feil, H.; Bae, Y. H.; Feijen, J.; Kim, S. W. Effect of comonomer hydrophilicity and ionization on the lower critical solution temperature of N-isopropylacrylamide copolymers. *Macromolecules* **1993**, *26*, 2496−2500.

(70) Weng, Y.; Ding, Y.; Zhang, G. Microcalorimetric Investigation on the Lower Critical Solution Temperature Behavior of N-Isopropycrylamide-co-Acrylic Acid Copolymer in Aqueous Solution. *J. Phys. Chem. B* **2006**, *110*, 11813−11817.

(71) Chee, C.-K.; Hunt, B. J.; Rimmer, S.; Rutkaite, R.; Soutar, I.; Swanson, L. Manipulating the thermoresponsive behavior of poly(N-isopropylacrlyamide) 3. On the conformational behaviour of N-isopropylacrylamide graft copolymers. *Soft Matter* **2009**, *5*, 3701−3712.

(72) Yim, H.; Kent, M. S.; Huber, D. L.; Satija, S.; Majewski, J.; Smith, G. S. Conformation of End-Tethered PNIPAM Chains in Water and in Acetone by Neutron Reflectivity. *Macromolecules* **2003**, *36*, 5244−5251.

(73) Plunkett, K. N.; Zhu, X.; Moore, J. S.; Leckband, D. E. PNIPAM Chain Collapse Depends on the Molecular Weight and Grafting Density. *Langmuir* **2006**, *22*, 4259−4266.

(74) Fan, Y.; Zhang, D.; Wang, J.; Jin, H.; Zhou, Y.; Yan, D. Preparation of Anion-Exchangeable Polymer Vesicles through the Self-Assembly of Hyperbranched Polymeric Ionic Liquids. *Chem. Commun.* **2015**, *51*, 7234−7237.

(75) Zhou, Y.; Yan, D.; Dong, W.; Tian, Y. Temperature-Responsive Phase Transition of Polymer Vesicles: Real-Time Morphology Observation and Molecular Mechanism. *J. Phys. Chem. B* **2007**, *111*, 1262−1270.

(76) Han, Q.; Chen, X.; Niu, Y.; Zhao, B.; Wang, B.; Mao, C.; Chen, L.; Shen, J. Preparation of Water-Soluble Hyperbranched Polyester Nanoparticles with Sulfonic Acid Functional Groups and Their Micelles Behavior, Anticoagulant Effect and Cytotoxicity. *Langmuir* **2013**, *29*, 8402−8409.

(77) Pamies, R.; Zhu, K.; Volden, S.; Kjoniksen, A.-L.; Karlsson, G.; Glomm, W. R.; Nystrom, B. Temperature-Induced Flocculation of Gold Particles with an Adsorbed Thermoresponsive Cationic Copolymer. *J. Phys. Chem. C* **2010**, *114*, 21960−21968.

(78) Karjalainen, E.; Chenna, N.; Laurinmäki, P.; Butcher, S. J.; Tenhu, H. Diblock Copolymers Consisting of a Polymerized Ionic

Liquid and Poly(N-isopropylacrylamide) . Effects of PNIPAM Block Length and Counter Ion on Self-Assembling and Thermal Properties. *Polym. Chem.* **2013**, *4*, 1014−1024.

(79) Blanazs, A.; Armes, S. P.; Ryan, A. J. Self-Assembled Block Copolymer Aggregates: From Micelles to Vesicles and their Biological Applications. *Macromol. Rapid Commun.* **2009**, *30*, 264−277.

(80) Holder, S. J.; Sommerdijk, N. A. J. M. New micellar morphologies from amphiphilic block copolymers: disks, toroids and bicontinuous micelles. *Polym. Chem.* **2011**, *2*, 1018−1028.

(81) Lombardo, D.; Kiselev, M. A.; Magazu, S.; Calandra, P. Amphiphilic Self-Assembly: Basic Concepts and Future Perspectives of Supramolecular Approaches. *Adv. Cond. Matter Phys.* **2015**, *2015*, 151683.

(82) Mai, Y.; Eisenberg, A. Self-assembly of block copolymers. *Chem. Soc. Rev.* **2012**, *41*, 5949−5985.

(83) Dai, Y.; Wang, H.; Zhang, X. Polyion complex micelles prepared by self-assembly of block-graft polycation and hyper-branched polyanion. *J. Nanopart. Res.* **2017**, *19*, 298.

(84) Brozowska, A.; Paczesny, J.; Parzuchowski, P.; Kusznerczuk, M.; Nikiforov, K.; Rokicki, G.; Gregorowicz, J. Hyperbranched Polyesters Terminated with Alkyl Chains of Different Length at the Air/Water Interface and on Solid Substrates. *Macromolecules* **2014**, *47*, 5256−5268.

(85) Liu, L.; Moon, K.-S.; Gunawidjaja, R.; Lee, E.; Tsukruk, V. V.; Lee, M. Molecular Reorganization of Paired Assemblies of T-Shaped Rod−Coil Amphiphilic Molecule at the Air−Water Interface. *Langmuir* **2008**, *24*, 3930−3936.

(86) Gonçalves da Silva, A. M.; Filipe, E. J. M.; d'Oliveira, J. M. R.; Martinho, J. M. G. Interfacial Behavior of Poly(styrene)-Poly-(ethylene oxide) Diblock Copolymer Monolayers at the Air-Water Interface. Hydrophilic Block Chain Length and Temperature Influence. *Langmuir* **1996**, *12*, 6547−6553.

(87) Zhang, J.; Cao, H.; Wan, X.; Zhou, Q. Molecular Reorganization of Rod-Coil Diblock Copolymers at the Air-Water Interface. *Langmuir* **2006**, *22*, 6587−6592.

(88) Peleshanko, P.; Jeong, J.; Gunawidjaja, R.; Tsukruk, V. V. Amphiphilic Heteroarm PEO-b-PS$_m$ Star Polymers at the Air-Water Interface: Aggregation and Surface Morphology. *Macromolecules* **2004**, *37*, 6511−6522.

(89) Pochan, D. J.; Gido, S. P.; Pispas, S.; Mays, J. W. Morphological Transitions in an I$_2$S Simple Graft Block Copolymer: From Folded Sheets to Folded Lace to Randomly Oriented Worms at Equilibrium. *Macromolecules* **1996**, *29*, 5099−5105.

(90) Namazu, T.; Isono, Y.; Tanaka, T. Evaluation of Size Effect on Mechanical Properties of Single Crystal Silicon by Nanoscale Bending Test Using AFM. *J. Microelectromech. Syst.* **2000**, *9*, 450−459.

(91) Sohn, Y.-S.; Park, J.; Yoon, G.; Song, J.; Jee, S.-W.; Lee, J.-H.; Na, S.; Kwon, T.; Eom, K. Mechanical Properties of Silicon Nanowires. *Nanoscale Res. Lett.* **2010**, *5*, 211−216.

(92) Shulha, H.; Zhai, X.; Tsukruk, V. V. Molecular Stiffness of Individual Hyperbranched Macromolecules at Solid Surfaces. *Macromolecules* **2003**, *36*, 2825−2831.

(93) Xiao, X.; Hu, J.; Charych, D. H.; Salmeron, M. Chain Length Dependence of the Frictional Properties of Alkylsilane Molecules Self-Assembled on Mica Studied by Atomic Force Microscopy. *Langmuir* **1996**, *12*, 235−237.

(94) Oishi, Y.; Umeda, T.; Kuramori, M.; Suehiro, K. Mechanical Properties of a Langmuir−Blodgett Film Measured by Atomic Force Microscopy. *Langmuir* **2002**, *18*, 945−947.

(95) Schmidt, S.; Zeiser, M.; Hellweg, T.; Duschl, C.; Fery, A.; Möhwald, H. Adhesion and Mechanical Properties of PNIPAM Microgel Films and Their Potential Use as Switchable Cell Culture Substrates. *Adv. Fucnt. Mat.* **2010**, *20*, 3235−3243.

(96) Lee, G.; Shin, Y.-H.; Son, J. Y. Formation of Self-Assembled Polyelectrolyte Multilayer Nanodots by Scanning Probe Microscopy. *J. Am. Chem. Soc.* **2009**, *131*, 1634−1635.

(97) Salerno, M.; El Merhie, A.; Diaspro, A.; Dante, S. Step-by-step surface potential tuning of patterned graphene by polyelectrolyte coating. *Thin Solid Films* **2018**, *660*, 253−257.

(98) Wu, Y.; Hayashi, K.; Saito, N.; Sugimura, H.; Takai, O. Imaging micropatterned organosilane self-assembled monolayers on silicon by means of scanning electron microscopy and Kelvin probe force microscopy. *Surf. Interface Anal.* **2003**, *35*, 94−98.